Chemistry–A European Journal
Research Article
doi.org/10.1002/chem.202301676
Chemistry Europe
European Chemical Societies Publishing
www.chemeurj.org

Hot Paper

Infrared Spectroscopic and Theoretical Investigations of Group 13 Oxyfluorides OMF_2 and OMF (M = B, Al, Ga, In)

Mei Wen,[a] Robert Medel,[a] Guohai Deng,[a] Yetsedaw A. Tsegaw,[a] Yan Lu,[a] and Sebastian Riedel*[a]

Group 13 oxyfluorides OMF_2 were produced by the reactions of laser-ablated group 13 atoms M (M=B, Al, Ga and In) with OF_2 and isolated in excess neon or argon matrices at 5 K. These molecules were characterized by matrix-isolation infrared spectroscopy and isotopic substitution experiments in conjunction with quantum-chemical calculations. The calculations indicate that the OMF_2 molecules have a $^2B_2$ ground state with C_{2v} symmetry. The computed molecular orbitals and spin densities show that the unpaired electron is mainly located at the terminal oxygen atom. Oxo monofluorides OMF were only observed in solid argon matrices and exhibit a linear structure in the singlet ground state. The M–O bonding in the OMF molecules can be rationalized as highly polar multiple bonds based on the calculated bond lengths and natural resonance theory (NRT) analyses. In particular, the molecular orbitals of OBF exhibit the character of a triple bond B–O resulting from two degenerate electron-sharing π bonds and an O→B dative σ bond formed by the oxygen 2p lone pair which donates electron density to the boron empty 2p orbital.

Introduction

Compounds featuring oxygen radical character are of fundamental importance as ubiquitous intermediates and prominent reactive oxygen species (ROSs) in, for example, chemistry, biology, and our atmosphere.[1–3] For instance, the alkoxy radicals (RO·), as crucial intermediates in organic synthesis,[4–7] undergo hydrogen atom transfer (HAT), β-scission, and additions onto unsaturation reactivities. The hydroxyl radicals (HO·) are involved in the oxidative damage and degradation of proteins induced by ROSs.[8] The oxy radicals of sulfur such as FSO_3·, FSO_5· and CH_3SO_3· exhibit significant effects on the Earth's sulfur cycle of the atmosphere.[9,10]

In addition to the aforementioned species, the structure and reactivity of oxygen radicals containing other main group elements have also been extensively investigated, such as the oxyhalide diatomic radicals XO· (X=halogen),[11–14] surface-bound siloxyl radicals (≡Si–O·)[15] as well as phosphate radicals ($-O_3PO$·).[16] To date, the majority of these oxygen radicals involve atoms of the group 14, 15, 16 and 17, while only a few examples involving group 13 atoms are known. The ·OBF_2, one of the few known group 13 molecules with terminal oxygen radical character, was observed for the first time from the emission spectrum produced by discharges through BF_3 and O_2 mixtures.[17] Subsequently, a series of theoretical calculations as well as laser-induced fluorescence (LIF) spectra ($\tilde{B}^2A_1 \rightarrow \tilde{X}^2B_2$ transition) have been reported about this unusual radical.[18–21] Recently, transition metal oxyfluoride species with the similar formula OMF_2 (M = transition metal) have been obtained by the reactions of transition metal atoms with OF_2 in cryogenic matrices.[22–24] Although most transition metal oxofluorides do not possess oxygen radical character, since transition metals readily form multiple M–O bonds involving d or f orbitals. Nevertheless, some transition metal oxyfluorides containing oxygen radicals have been identified using matrix-isolation IR spectroscopy supported by electronic structure calculation, including OMF_2 with C_{2v} structure in $\tilde{X}^2B_2$ ground states (M=Sc, Y and La),[25,26] and OMF_2 with T-shape structure in $\tilde{X}^3A_2$ ground states (M=Ni, Pd and Pt).[27]

Inspired by the formation of transition metal oxyfluoride radical species, herein we report the novel group 13 oxofluoride radicals ·OMF_2 (M=B, Al, Ga and In) by using laser-ablated B, Al, Ga and In atoms reacted with OF_2 and isolated in solid neon and argon matrices. The spin-density and molecular orbitals (MOs) profiles confirmed that the unpaired electron is centered on the oxygen atom of the OMF_2 molecules. In addition, the infrared experiments in argon matrices revealed the existence of OMF molecules. The MOs and the natural resonance theory (NRT) calculations show that OBF, OAlF and OGaF possess each an M–O (M=B, Al and Ga) triple bond character. In contrast, the heavier analog OInF has a highly polar double bond interaction between the In and O atoms. We also briefly discuss the possibility of formation of the unusual peroxo dimer $F_2Al(\mu\text{–}\eta^2\text{:}\eta^2\text{–}O_2)AlF_2$ from the $OAlF_2$ radical in our experiments, based on the reported calculations.[28]

[a] M. Wen, Dr. R. Medel, Dr. G. Deng, Dr. Y. A. Tsegaw, Y. Lu, Prof. Dr. S. Riedel
Freie Universität Berlin
Institut für Chemie und Biochemie-Anorganische Chemie
Fabeckstrasse 34/36, 14195 Berlin (Germany)
E-mail: s.riedel@fu-berlin.de

Supporting information for this article is available on the WWW under https://doi.org/10.1002/chem.202301676

Experimental and Computational Methods

The group 13 oxyfluoride products were generated by the reactions of laser-ablated B, Al, Ga and In atoms and $^{16}OF_2$ or $^{18}OF_2$ in excess neon or argon onto a cryogenic CsI window (for Al, Ga and In) or onto a gold plated copper mirror (for B) and cooled to 5 K by using a closed-cycle helium cryostat (Sumitomo Heavy Industries, RDK-205D) inside a vacuum chamber. The experimental apparatus and procedure have been described in detail in previous studies.[29,30] Briefly, the 1064 nm fundamental of a Nd:YAG laser (Continuum, Minilite II) with a pulse energy of 50–65 mJ per 10 ns pulse was focused on the elemental group 13 targets through a hole in the cold window. $^{16/18}OF_2$ was synthesized by a known procedure using elemental fluorine and $^{16/18}OH_2$ dispersed in solid NaF.[31] FTIR spectra were recorded on a Bruker Vertex 80v spectrometer for B and Bruker Vertex 70 spectrometer for Al, Ga and In at 0.5 cm^{-1} resolution in the 4000–430 cm^{-1} region using an MCT detector. The matrix samples were irradiated by an LED light (OSLON 80 4+ PowerStar Circular 4 LED Arrays: $\lambda = 470 \pm 20$ nm, 13 W) or a mercury arc lamp (Osram HQL 250, 175 W) with the outer globe removed.

All calculations were carried out using the Gaussian 16 program package.[32] The electronic structure and vibrational frequencies were calculated by means of the hybrid density functionals including dispersion corrections like B3LYP–D3.[33,34] In addition, high-level quantum-chemical calculations at the CCSD (coupled-cluster singles-doubles)[35] level were also performed. Additional CCSD(T) (coupled-cluster singles-doubles with perturbational triples excitations)[36,37] calculations were carried out to obtain more accurate results for electronic structure information. For all calculations, Dunning's correlation consistent polarized basis sets of triple-zeta quality with diffuse augmentation functions (aug-cc-pVTZ) were used for B, O, F and Al atoms, aug-cc-pVTZ-PP[38–40] with scalar-relativistic effective core pseudopotentials (ECP) were used for Ga and In atoms. The natural resonance theory (NRT) analyses and natural population analysis (NPA) were carried out at the B3LYP/aug-cc-pVTZ-PP level using the NBO 7.0 program.[41] The molecular orbitals were visualized using the program Chemcraft.[42]

Results and Discussion

Experimental Results

Boron Spectra

The infrared spectra from co-deposited laser-ablated ^{10}B-enriched boron (>95%) with 0.05% $^{16}OF_2$ or $^{18}OF_2$ in neon at 5 K are presented in Figure 1. Vibrational signatures of boron fluorides $^{10}BF_n$ ($n = 1$–3) were observed after 30 min deposition, at almost the same positions as obtained before from the reaction of boron atoms and F_2.[43] No obvious boron oxide compounds were observed. The absorptions at 521.4 and 2148.6 cm^{-1} that appeared after co-deposition were assigned to $O^{10}BF$ in the previous work[44] and showed no obvious growth on full-arc mercury lamp photolysis ($\lambda > 220$ nm).

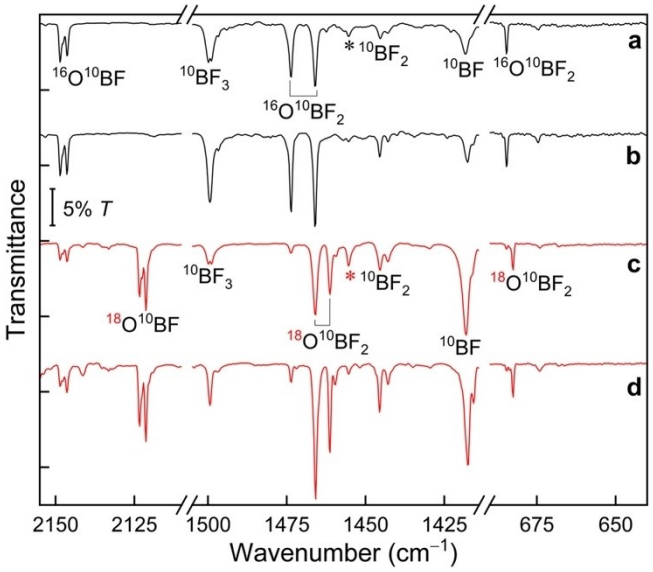

Figure 1. Infrared spectra of the reaction products obtained from laser-ablated ^{10}B-enriched boron (>95%) with OF_2 in excess of Ne at 5 K: **a** ^{10}B + 0.05% OF_2/Ne co-deposition for 30 min, **b** after irradiation with $\lambda > 220$ nm for 15 min, **c** ^{10}B + 0.05% $^{18}OF_2$/Ne co-deposition for 30 min, and **d** after irradiation with $\lambda > 220$ nm for 15 min. Unassigned bands are marked by an asterisk.

In addition to these known absorptions, new absorptions at 684.6, 1466.0 and 1473.9 cm^{-1} increased in intensity concurrently upon irradiation with $\lambda > 220$ nm. This set of absorptions shifted to 658.0, 1416.2 and 1423.9 cm^{-1} in the natural boron isotope abundance experiment (80.4% ^{11}B, 19.6% ^{10}B) (Figure S1), providing doublet distributions for each mode with 1:4 intensity ratio, which indicate that only one boron atom is involved in these modes. These bands were observed neither after the reaction of boron with O_2 nor after the interaction of BF_3 with excited neon atoms,[43,44] suggesting that they originate from a ternary boron oxyfluoride. The band at 1466.0 cm^{-1} appeared in the B–F stretching region and exhibited no $\Delta\nu(^{16/18}O)$ isotope shift. Hence, we assign this band to the antisymmetric F–^{10}B–F stretching mode. Whereas the 1473.9 cm^{-1} band exhibited a 12.4 cm^{-1} oxygen isotopic shift and a 50.0 cm^{-1} boron isotopic shift and belongs therefore to the ^{10}B–O stretching mode. A small $\Delta\nu(^{16/18}O)$ isotope shift of 2.0 cm^{-1} was found for the lower 684.6 cm^{-1} absorption, indicating that it is likely to be an out-of-plane bending mode in which oxygen is not strongly involved. Based on these assignments, the new compound is identified as OBF_2. All these bands of OBF_2 and OBF molecules were also observed in solid argon (see Supporting Information Figures S2 and S3).

Aluminum Spectra

Figure 2 displays the infrared spectra for the products formed upon reactions of laser-ablated aluminum atoms with 0.05%

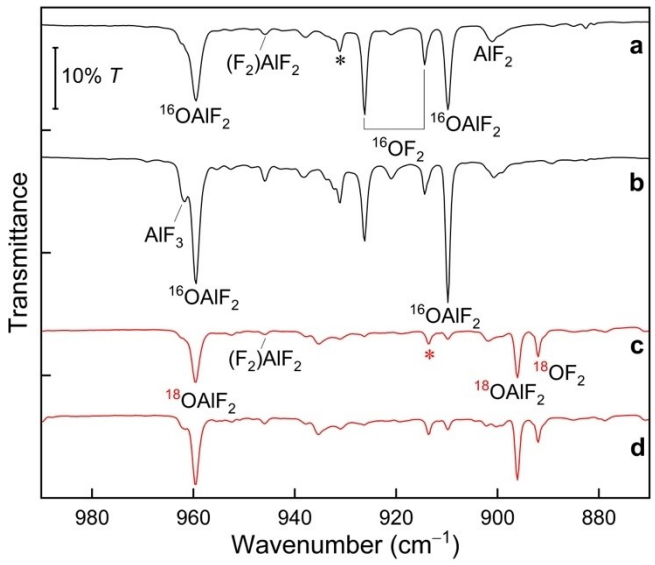

Figure 2. Infrared spectra of the reaction products obtained from laser-ablated aluminum atoms with OF_2 in excess of neon at 5 K: **a** Al + 0.05 % OF_2/Ne co-deposition for 90 min, **b** after irradiation with $\lambda > 220$ nm for 15 min, **c** Al + 0.05 % $^{18}OF_2$/Ne co-deposition for 90 min, and **d** after irradiation with $\lambda > 220$ nm for 15 min.

$^{16}OF_2$ or $^{18}OF_2$ in solid neon matrices. The identified species are compiled in Table 1. Based on the previously published results on the reaction of aluminum with F_2,[45] the broad bands at 786.0, 901.1, 961.9 and 945.8 cm^{-1} were assigned to the AlF, AlF_2, AlF_3 and the high electron affinity neutral molecule $(F_2)AlF_2$, respectively. In addition, new product absorptions at 909.8 and 959.5 cm^{-1} were observed after 90 min deposition, with some partial overlap between the 959.5 cm^{-1} band and AlF_3 molecular absorption. These two new bands significantly increased upon subsequent irradiation with $\lambda > 220$ nm and their relative intensities remained constant. Therefore, these two new absorptions should be different vibrational modes of the same aluminum species. Furthermore, the overlapping bands at 959.5 and 961.9 cm^{-1} can be distinguished easily from the spectrum after irradiation with $\lambda > 220$ nm (Figure 2, trace b). To identify the new products, a similar experiment was carried out using the $^{18}OF_2$ sample under the same conditions (Figure 2, trace c). The behavior of the new band at 896.1 cm^{-1} during UV irradiation was almost identical to the one observed at 909.8 cm^{-1} in the $^{16}OF_2$ experiment (Figure 2, trace d). The corresponding larger 13.7 cm^{-1} oxygen isotopic shift suggest it should be the Al–O stretching mode. Since no ^{18}O shift was observed for the 959.5 cm^{-1} band and the absorption appeared in a region of aluminum fluorides absorption, it can be assigned to the F–Al–F antisymmetric stretching mode. Hence, this group absorptions are appropriate for the $OAlF_2$ molecule. Apart from these assigned bands, there are absorptions of an unknown species with an 18.3 cm^{-1} $\Delta\nu(^{16/18}O)$ isotope shift that appeared in a region where aluminum fluoride stretching vibrations absorb, denoted with asterisks in Figure 2. They slightly increased upon $\lambda > 220$ nm, which might originate from the dimer $F_2Al(\mu\text{–}\eta^2\text{:}\eta^2\text{–}O_2)AlF_2$ based on the values previously reported by quantum-chemical calculations.[28]

The Al–O stretch and antisymmetric F–Al–F stretch of $OAlF_2$ were also detected in the argon deposit (see Supporting Information Figure S4 and Table 1). Additionally, the oxo monofluoride OAlF was observed at 1147.9 cm^{-1} in an argon matrix experiment (Figure S4), which is consistent with the reported position (1148 cm^{-1}) by co-condensation of AlF with oxygen atoms under cryogenic conditions in argon matrices.[46] The in-phase O–Al–F stretching band was not detected experimentally, which is in line with its calculated low infrared intensity (Table 1). No apparent growth of OAlF absorption was observed upon further irradiation (Figure S4, trace b and d).

Gallium Spectra and Indium Spectra

Figure 3 shows the infrared spectra from co-deposited gallium atoms (^{69}Ga and ^{71}Ga, 60.1 and 39.9 %, respectively, in natural abundance) with 0.05 % $^{16}OF_2$ or $^{18}OF_2$ in neon. The broad bands of GaF and GaF_2 were observed at 607.1 and 685.0 cm^{-1}, respectively, which are consistent with the previous identifications.[45] New absorptions were resolved at 740.5 and 746.8 cm^{-1} and the corresponding gallium isotopic bands were partially resolved at 737.8 and 744.0 cm^{-1}. These new bands tracked together as they greatly increased upon subsequent LED irradiation ($\lambda = 470$ nm). The doublet gallium isotopic splitting's clearly show that the new species has a single gallium atom. Furthermore, the experiment of gallium with $^{18}OF_2$ was also performed to further aid our assignment. Doublet feature peaks at 740.5 and 737.8 cm^{-1} undergo 11.5 and 11.3 cm^{-1} oxygen shift, respectively, as illustrated in Figure 2 (trace c and d). The band positions and the oxygen isotopic shift confirmed the presence of a symmetric F–Ga–F stretching mode coupled with the Ga–O stretching mode. The 746.8/744.0 cm^{-1} bands

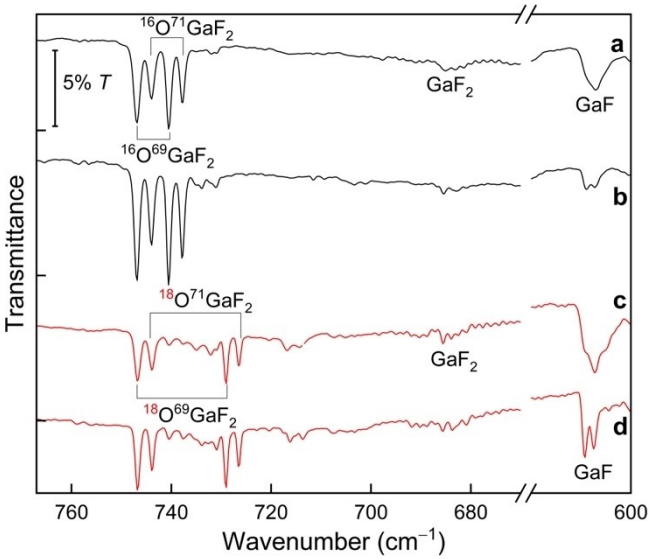

Figure 3. Infrared spectra of the reaction products obtained from laser-ablated gallium atoms with OF_2 in excess of neon at 5 K: **a** Ga + 0.05 % OF_2/Ne co-deposition for 60 min, **b** after irradiation with $\lambda = 470 \pm 20$ nm for 15 min, **c** Ga + 0.05 % $^{18}OF_2$/Ne co-deposition for 60 min, and **d** after irradiation with $\lambda = 470 \pm 20$ nm for 15 min.

Table 1. Selected experimental and calculated normal mode wavenumbers and their $^{16/18}O$ isotope shifts $\Delta\nu$ (in cm^{-1}) for the group 13 oxyfluorides.

	Exp.(Ne matrix)			Exp.(Ar matrix)			CCSD(T)[a]		
molecule	$\nu(^{16}O)$	$\nu(^{18}O)$	$\Delta\nu$	$\nu(^{16}O)$	$\nu(^{18}O)$	$\Delta\nu$	$\nu(^{16}O)$	$\Delta\nu$	stretching mode
$O^{10}BF$	521.4	517.7	3.7	513.9	510.3	3.6	516.5 (73)	3.7	O–^{10}B–F bend
	2148.6	2123.3	25.3	2136.1	2111.6	24.5	2164.8 (408)	25.0	^{10}B–O mix[b]
$O^{11}BF$	502.7	499.0	3.7	495.4	491.7	3.7	498.1 (68)	3.9	O–^{11}B–F bend
	2077.5	2050.8	26.7	2064.8	2038.9	25.9	2090.3 (377)	26.1	^{11}B–O mix[b]
$O^{10}BF_2$	684.6	682.6	2.0	675.9	673.9	2.0	690.4 (83)	2.1	out-of-plane bending
	1473.9	1461.5	12.4	1466.2	1454.0	12.2	1497.8 (405)	12.6	^{10}B–O
	1466.0	1466.0	0.0	1458.9	1458.9	0.0	1498.3 (276)	0.0	antisym. F–^{10}B–F
$O^{11}BF_2$	658.0	656.0	2.0	649.8	647.7	2.1	663.6 (77)	2.2	out-of-plane bending
	1423.9	1410.7	13.2	1416.8	1403.9	12.9	1445.6 (374)	13.1	^{11}B–O
	1416.2	1416.1	0.1	1409.5	1409.3	0.2	1446.5 (254)	0.0	antisym. F–^{11}B–F
OAlF	–[c]	–[c]	–[c]	–[c]	–[c]	–[c]	732.5 (21)	16.3	Al–F mix[b]
	–[c]	–[c]	–[c]	1147.9	1124.2	23.7	1143.9 (104)	23.4	Al–O mix[b]
$OAlF_2$	–[c]	–[c]	–[c]	–[c]	–[c]	–[c]	674.4 (0)	15.3	Al–O mix[d]
	909.8	896.1	13.7	895.3	882.6	12.7	905.5 (140)	12.5	sym. F–Al–F mix[d]
	959.5	959.5	0.0	946.4	946.4	0.0	950.1 (180)	0.4	antisym. F–Al–F
$O^{69}GaF$	–[c]	–[c]	–[c]	690.2	681.1	9.1	696.9 (37)	9.0	^{69}Ga–F mix[b]
				943.1	909.7	33.4	952.9 (68)	34.0	^{69}Ga–O mix[b]
$O^{71}GaF$	–[c]	–[c]	–[c]	690.2	681.1	9.1	696.1 (38)	8.9	^{71}Ga–F mix[b]
				939.4	905.9	33.5	949.0 (66)	34.3	^{71}Ga–O mix[b]
$O^{69}GaF_2$	–[c]	–[c]	–[c]	–[c]	–[c]	–[c]	664.8 (1)	20.0	^{69}Ga–O mix[d]
	740.5	729.0	11.5	733.1	719.2	13.9	745.8 (76)	12.9	sym. F–^{69}Ga–F mix[d]
	746.8	746.7	0.1	736.1	736.0	0.1	750.1 (107)	0.1	antisym. F–^{69}Ga–F
$O^{71}GaF_2$	–[c]	–[c]	–[c]	–[c]	–[c]	–[c]	664.8 (1)	20.1	^{71}Ga–O mix[d]
	737.8	726.5	11.3	727.8	716.6	11.2	743.0 (75)	12.5	sym. F–^{71}Ga–F mix[d]
	744.0	743.9	0.1	730.4	730.4	0.0	746.9 (106)	0.3	antisym. F–^{71}Ga–F
OInF	–[c]	–[c]	–[c]	598.4	592.8	5.6	603.9 (46)	6.2	In–F mix[b]
	–[c]	–[c]	–[c]	782.6	750.2	32.4	785.3 (58)	32.4	In–O mix[b]
$OInF_2$	–[c]	–[c]	–[c]	–[c]	–[c]	–[c]	583.2 (0)	22.8	In–O mix[d]
	631.5	625.7	5.8	619.9	613.4	6.5	625.9 (69)	5.1	sym. F–In–F mix[d]
	628.5	628.4	0.1	614.9	614.9	0.0	627.1 (95)	0.7	antisym. F–In–F

[a] values obtained at the CCSD(T)/aug-cc-pVTZ-PP level with B3LYP–D3 intensities (in km/mol) in parentheses using the Gaussian 16 program. [b] The M–O stretches mix with the M–F stretches. [c] Bands not observed, or too weak. [d] The M–O stretches mix with the symmetric F–M–F stretches. More calculated frequencies are shown in Supporting Information Table S1.

with the strong doublet feature were designated to the asymmetric F–Ga–F stretching mode based on almost no oxygen-18 shift and due to their absolute band positions. In summary, we assign these new bands to $O^{69}GaF_2$ (740.5 and 746.8 cm^{-1}) and $O^{71}GaF_2$ (737.8 and 744.0 cm^{-1}) molecules. Likewise, $O^{69}GaF_2$ and $O^{71}GaF_2$ molecules were also observed in argon matrices (see Figure S5, Table 1). Furthermore, $O^{69}GaF$ (690.2 and 943.1 cm^{-1}) and $O^{71}GaF$ (690.2 and 939.4 cm^{-1}) were only observed in argon matrices, in agreement with the earlier findings.[47]

Following the boron, aluminum and gallium experiments, the spectra obtained from the reactions of indium atoms and OF_2 in solid neon matrices are shown in Figure 4. $OInF_2$ absorbed at 628.5 and 631.5 cm^{-1} (Figure 4, trace a). The 628.5 cm^{-1} band is reasonably attributed to the antisymmetric F–In–F based on the lack of a $^{16/18}O$ isotopic shift and its absolute position. However, the 631.5 cm^{-1} band showed a small $^{16/18}O$ isotopic shift of 5.8 cm^{-1} in the ^{18}O substitution experiments (Figure 4, trace c), suggesting that this band should be assigned to the F–In–F symmetric stretching vibrational mode coupled with the In–O stretch. $OInF_2$ absorptions found in solid argon matrices during the reactions of In atoms and OF_2 are given in Table 1 and the spectra are shown in Figure S6. Besides, it is evident that there is a second set of absorptions at 598.4 and 782.6 cm^{-1} during sample deposition in Figure S6. No growth was observed for this group absorp-

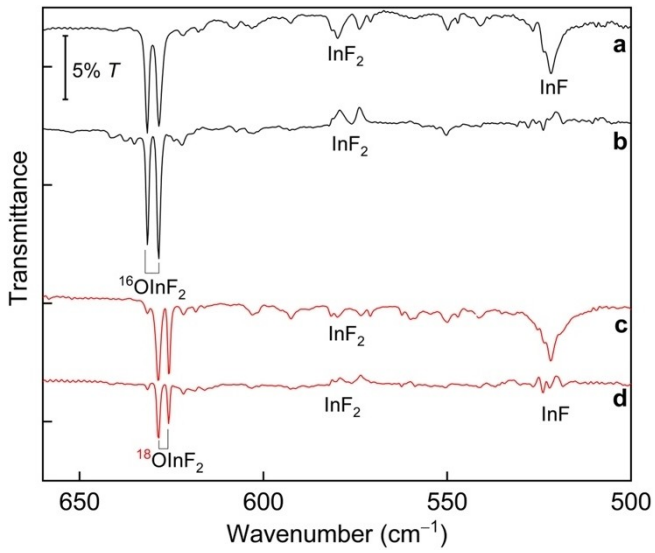

Figure 4. Infrared spectra of the reaction products obtained from laser-ablated indium with OF_2 in excess of neon at 5 K: **a** In + 0.05 % OF_2/Ne co-deposition for 110 min, **b** difference spectrum after irradiation with λ > 220 nm for 15 min, **c** In + 0.05 % $^{18}OF_2$/Ne co-deposition for 110 min, and **d** difference spectrum after irradiation with λ > 220 nm for 15 min.

tions upon subsequent UV photolysis. The experiment with an $^{18}OF_2$ sample, shows a band at 598.4 cm^{-1} with a small $^{16/18}O$ isotopic shift of 5.6 cm^{-1}, which was assigned to the In–F stretch which is slightly coupled with the In–O stretch. The higher band at 782.6 cm^{-1} exhibited an quite large $^{16/18}O$ isotopic shift of 32.4 cm^{-1}, which confirmed the presence of a terminal In–O bond similar to that in the linear OInO structure.[48] Thus, the two new bands are assigned to the OInF molecule.

Computational Results

Quantum-chemical calculations at the B3LYP–D3, CCSD and CCSD(T) methods using the aug-cc-pVTZ-PP basis set have been performed to optimize the molecular structures and compute their corresponding vibrational frequencies. The oxydifluorides OMF_2 (M=B, Al, Ga and In) show C_{2v} symmetry with an $^2B_2$ electronic ground state. The OMF molecules are all computed to possess linear structures in the $^1\Sigma^+$ electronic ground state. Table 2 lists the corresponding calculated structural parameters. The CCSD and B3LYP–D3 normal mode analyses are summarized in Table S1.

For $O^{10}BF_2$, the calculated harmonic frequencies at the DFT level are coincidentally closer to experimental fundamental values than the calculated results at the CCSD and CCSD(T) levels. The DFT frequency calculations predict the strong F–^{10}B–F antisymmetric stretching mode at 1455.9 cm^{-1}, the ^{10}B–O stretching mode at 1467.9 cm^{-1} and the out-of-plane bending mode at 679.6 cm^{-1}, which exhibit only 0.7 %, 0.4 % and 0.7 % differences, respectively, compared to the observed results in neon matrices. The corresponding CCSD and CCSD(T) values are higher by about 44 and 24 cm^{-1}, respectively, for the

Table 2. Optimized Structures of OMF and OMF_2.

	CCSD(T)/aug-cc-pVTZ-PP		
molecule	M–O (Å)	M–F (Å)	∠FMO (deg)
OBF ($C_{\infty v}$, $^1\Sigma^+$)	1.217	1.289	180.0
OAlF ($C_{\infty v}$, $^1\Sigma^+$)	1.616	1.646	180.0
OGaF ($C_{\infty v}$, $^1\Sigma^+$)	1.648	1.708	180.0
OInF ($C_{\infty v}$, $^1\Sigma^+$)	1.850	1.918	180.0
OBF_2 (C_{2v}, $^2B_2$)	1.370	1.318	119.3
$OAlF_2$ (C_{2v}, $^2B_2$)	1.741	1.644	119.1
$OGaF_2$ (C_{2v}, $^2B_2$)	1.786	1.723	120.6
$OInF_2$ (C_{2v}, $^2B_2$)	1.999	1.935	121.7

^{10}B–O stretching band if compared with the experiment. As compiled in Table 1, the corresponding calculated $\Delta\nu(^{16/18}O)$ shift for ^{10}B–O stretching of 12.6 cm^{-1} at the CCSD(T) level is close to the experimentally observed value of 12.4 cm^{-1}. As seen in Table S1, the calculated $\Delta\nu(^{16/18}O)$ shifts for the ^{10}B–O stretching at the CCSD and DFT levels are also in good agreement with experiment. Furthermore, the calculated harmonic wavenumbers at the CCSD(T) level for the boron isotopolog $O^{11}BF_2$ are 663.6, 1455.6 and 1446.5 cm^{-1}, showing 26.8, 52.2 and 51.8 cm^{-1} boron isotopic shift, respectively, are in good agreement with the experimentally observed boron shifts of 26.6, 49.8 and 50.0 cm^{-1}. Besides, the calculated ^{10}B–O and O–^{10}B–F stretching wavenumbers for oxo monofluoride $O^{10}BF$ at the CCSD(T) level of theory are 2164.8 and 516.5 cm^{-1}, respectively, which are in reasonable accordance with the experimental values in neon matrix (2148.6 and 521.4 cm^{-1}).

For the $OAlF_2$ product, the calculated Al–O stretching and antisymmetric ν_{as}(F–Al–F) stretching vibrational wavenumbers at the CCSD(T) level are 905.5 and 950.1 cm^{-1}, respectively, which are more in accordance with the absorptions observed at 909.8 and 959.5 cm^{-1} in neon matrix than the B3LYP–D3 and CCSD results. The calculated Al–O stretching at the CCSD(T) level shows a 12.5 cm^{-1} oxygen isotopic shift, in line with the experimentally observed shift of 13.7 cm^{-1}. The calculated frequencies and $\Delta\nu(^{16/18}O)$ shifts of the $OAlF_2$ molecule at the B3LYP–D3 and CCSD levels are in qualitative agreement with experiment. At the CCSD(T) level, another product OAlF is predicted at 1143.9 (Al–O stretching) and 732.5 cm^{-1} (O–Al–F stretching) with $^{16/18}O$ isotopic shift of 23.4 and 16.3 cm^{-1}, respectively. The former is consistent with the experimental observed Al–O stretching oxygen isotopic shift of 23.7 cm^{-1}. Notably, the experimental values of asterisk-marked absorptions at 931.9 cm^{-1} in Figure 2 are inconsistent with the calculated wavenumbers of $F_2Al(\mu\text{–}\eta^2\text{:}\eta^2\text{–}O_2)AlF_2$ dimer (see Supporting Information Table S2).

DFT calculations of the gallium oxydifluoride $OGaF_2$ show frequencies which are too low for the Ga–F stretches. The CCSD(T) calculated symmetric and antisymmetric Ga–F stretching frequencies of $O^{69}GaF_2$ are 745.8 and 750.1 cm^{-1}, respectively, which is in good agreement with the observed bands at 740.5 and 746.8 cm^{-1} in neon matrix. In accordance with

gallium isotopic splitting's, the 737.8 and 744.0 cm^{-1} bands are due to $O^{71}GaF_2$. The Ga–O stretching mode of the OGaF molecule is too weak to be observed in our experiments. For $O^{69}GaF_2$, the predicted oxygen isotope shifts for symmetric and antisymmetric F–Ga–F stretching at the CCSD(T) level are 12.9 cm^{-1} and 0.1 cm^{-1}, respectively, which are in good agreement with corresponding experimental results of 11.5 and 0.1 cm^{-1} using ^{18}O enriched OF_2 in neon. The calculated wavenumber values of O–^{69}Ga–F (696.9 cm^{-1}) and ^{69}Ga–O (952.9 cm^{-1}) vibration modes in the $O^{69}GaF$ molecule at the CCSD(T) level are close to the observed positions at 690.2 and 943.1 cm^{-1} in argon, respectively.

For $OInF_2$, the calculated CCSD(T) antisymmetric F–In–F stretch at 627.1 cm^{-1} and the symmetric F–In–F stretch at 625.9 cm^{-1} (In–F stretching mode coupled with the In–O stretch) match with the experimental observed absorptions at 628.5 and 631.5 cm^{-1} in neon matrices, respectively. In addition, the observed isotopic oxygen shift of 5.8 cm^{-1} for absorption at 631.5 cm^{-1} in neon is in accordance with the theoretically predicted isotopic oxygen shift of 5.1 cm^{-1} for the band at 625.9 cm^{-1}. The calculated $^{16/18}O$ isotopic shifts for the symmetric F–In–F stretch at the B3LYP–D3 and CCSD levels are also in agreement with the experiment. CCSD(T) calculations of the oxo monofluoride OInF, show an In–F stretching slightly coupled with the In–O stretching mode (O–In–F) which is ~5 cm^{-1} higher than the experimental value, and the In–F stretch is predicted to be ~3 cm^{-1} higher than the experimental value. Furthermore, our calculations show In–F and In–O stretching modes which are 6.2 and 32.4 cm^{-1} red shifted upon ^{18}O substitution, which is consistent with the corresponding observed shifts of 5.6 and 32.4 cm^{-1}. The CCSD and DFT values are in agreement with experiment for the O–In–F (within 20 cm^{-1}) and In–O stretches (within 10 cm^{-1}).

Bonding Situations

The bond lengths and angles for the global minimum structure of OMF_2 and OMF (M=B, Al, Ga and In) molecules are given in Table 2. The calculated M–O bond lengths at the CCSD(T) level are in good agreement (within 0.1 Å) with those at the CCSD and B3LYP–D3 levels (see Table S3). The molecular orbitals (MOs) visualization below can be used to further illustrate the nature of M–O bonds in OMF_2 and OMF (M=B, Al, Ga and In) molecules.

In this work, OMF_2 molecules are the main observed products, the data in Table 2 suggests that the M–O bond lengths in OMF_2 are considerably longer than in OMF. The calculated B–O bond length at the CCSD(T) level in OBF_2 is 1.370 Å, which is close to the B–O single-bond length of 1.352 Å in, for example, H_2BOH.[49] The Al–O distance of 1.741 Å in the $OAlF_2$ is the typical Al–O single-bond distance observed in 4-coordinate aryloxide compounds.[50] The Ga–O (1.786 Å) and In–O (1.999 Å) bond lengths in $OGaF_2$ and $OInF_2$ molecules are significantly longer than the reported Ga=O (1.70 Å) and In=O (1.82 Å) double bond lengths.[48] To investigate the detailed bonding situation, we have analyzed the electronic configuration of OMF_2. Herein, taking $OInF_2$ as an example. The electronic configuration of $OInF_2$ with C_{2v} symmetry in the $^2B_2$ ground state has the following HOMOs with increasing energy: $11a_1$ σ bond orbital, $4b_1$ oxygen 'out-of-plane lone pair' nonbonding orbital, and $7b_2$ oxygen 'in-plane open shell p' nonbonding orbital [the single occupied orbital (SOMO)] which involves the In 5p and O 2p orbitals (Figure 5). The plots of the molecular orbitals reveal the single radical characteristics of the terminal oxygen atom of the $OInF_2$ molecule, which can be further identified by the computed spin density (Figure S9) located at the oxygen atom (1.037 e). The analogous MOs and computed spin density of OBF_2, $OAlF_2$ and $OGaF_2$ molecules are displayed in Figure S7 and Figure S9.

Although OBF, OAlF and OGaF have been generated previously using different reactions, the bond properties of these species were not described in detail. Compared with OMF_2, OMF has a significantly shorter M–O bond length and a higher M–O stretching frequency, indicating a stronger M–O bond.

For the OBF molecule, the calculated B–O bond length (1.217 Å) at the CCSD(T) level is close to the sum of the reported boron oxygen triple bond radii (1.21 Å) in the single crystal structure of oxoboryl complex trans-[$(Cy_3P)_2BrPt(B{\equiv}O)$] (Cy being cyclohexyl).[51] The iso(valence) electronic molecules of O≡BF, acetonitrile compound analog H_3CBO, also shows a B≡O triple bond character.[52] Complex trans-[$(Cy_3P)_2BrPt(^{10}B{\equiv}O)$] and $H_3C^{10}B{\equiv}O$ show IR absorption bands at 1853 and 1907.5 cm^{-1}, respectively, yet $O{\equiv}^{10}B$–F has a significantly higher wavenumber (2148.6 cm^{-1} in neon), which is indicative for a stronger B≡O triple bond character in OBF. Figure 6 presents the OBF resonance structures[53] and the MOs of OBF are shown in Figure 7.

The natural resonance theory (NRT) calculations show that the O≡B–F form has an 89% weight. Furthermore, the NRT bond index of 2.91 further suggests a triple bond character between boron and oxygen. Therefore, the OBF compound involves a triple bond derived from two degenerate electron-sharing π bonds and an O→B dative σ bond formed by the oxygen 2p lone pair electrons donating to the boron 2p empty orbital.

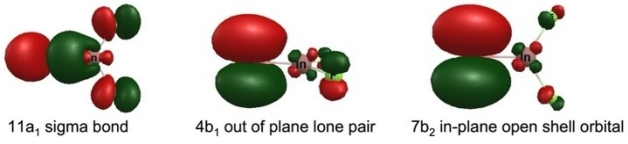

Figure 5. Molecular orbitals (MOs) for $OInF_2$ computed at the B3LYP–D3/aug-cc-pVTZ-PP level of theory.

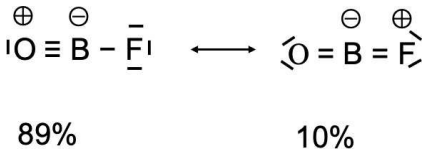

Figure 6. Major Lewis resonance structures of OBF as predicted by natural resonance theory (NRT).

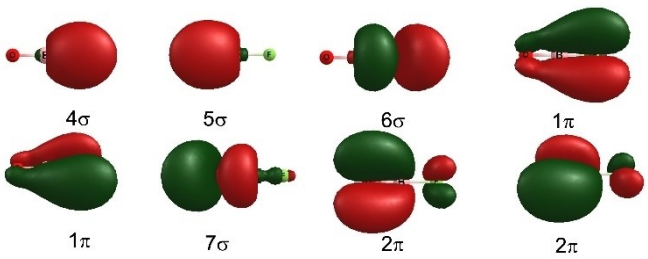

Figure 7. Molecular orbitals (MOs) of OBF computed at the B3LYP–D3/aug-cc-pVTZ level of theory. The atoms from left to right are O, B and F.

For aluminum, the CCSD(T) calculated Al–O bond length of 1.616 Å in the OAlF compound is significantly shorter than both the predicted sum of the molecular covalent double bond radii (1.70 Å) and the Lewis acid stabilized "Al=O" bond (1.659 Å) experimentally determined in the [Al-(NONAr)(O)]$^-$ anion.[54] NRT analyses of the electronic structure of OAlF molecule revealed a highly polar Al–O triple bond character with a 79% ionic contribution to the NRT Al–O bond order of 2.97. The high polarity of the Al–O bond is also reflected in the high opposite natural population analysis (NPA) charges (O, −1.34; Al, +2.09) compiled in Table 3.

The Ga–O bond length (1.648 Å) in OGaF with 2.91 NRT bond index is significantly shorter than the one in linear OGaO molecule (1.70 Å) with 1.6 bond order.[48] Thus, the Ga–O bond in OGaF appears to be best described as a triple bond. In contrast, for the indium oxo monofluorides OInF, the calculated In–O bond length (1.850 Å) with the CCSD(T) method is close to the In–O bond length of the reported linear OInO molecule (1.82 Å) in the $^2\Pi_g$ ground state.[48] The In–O bond order in the linear OInO molecule was estimated as 1.6 according to the formula introduced by Siebert,[55] which is similar to our calculated In–O double NRT bond index of 1.94 with 31% covalent contribution and 69% ionic contribution for OInF. Therefore, the In–O bond in the OInF can be described as a highly polar double bond.

The MOs for Al, Ga and In analogs are provided in Figure S8 in the Supporting Information. The M–O bonding orbitals are localized more on oxygen than on group 13 elements, which also reflects the polarity of this interaction. The two degenerate π bonding interactions with the *n*p (*n* = 3, 4, 5) orbitals of Al, Ga and In are weaker than with the 2p orbitals of B, explaining their weaker covalent bonding character.

Reaction Energies

The reaction energies computed at the CCSD(T) level are listed in Table 4. The reaction pathway for the formation of OMF_2 (M=B, Al, Ga and In) molecules are shown in reaction (1). The formation processes are for all compounds (B, Al, Ga, In) computed to be highly exothermic by 327.9, 276.1, 210.5 and 169.1 kcal/mol, respectively (Table 4). Thus, boron, aluminum, gallium, and indium atoms are likely to react directly with OF_2.

$$M + OF_2 \rightarrow OMF_2 \quad (1)$$

There are two reasonable reaction routes for the formation of triatomic OMF molecules [reaction (2) and reaction (3)]. Reaction (2) describes the formation of OMF upon the reactions of group 13 atoms and OF radicals. The single-point energy calculations at the CCSD(T) level reveal that the reaction (2) is highly exothermic by −293.6, −201.5, −162.1 and −129.3 kcal/mol for B, Al, Ga and In, respectively. OF radicals might be

Table 3. Selected B3LYP-calculated results of NRT analyses and NPA charges.

	NRT analysis			NPA Charges		
	Bond order b_{O-M}	Covalent Bond order[a]	Ionic Bond order[a]	O	M	F
OBF	2.91	1.14 (39%)	1.77 (61%)	−0.83	+1.27	−0.43
OAlF	2.97	0.63 (21%)	2.35 (79%)	−1.34	+2.09	−0.74
OGaF	2.91	0.74 (25%)	2.18 (75%)	−1.14	+1.81	−0.68
OInF	1.94	0.61 (31%)	1.34 (69%)	−1.14	+1.85	−0.71

[a] The percentages within the parentheses show the contributions towards the total bond. Basis sets: aug-cc-pVTZ for B, O, F, Al; aug-cc-pVTZ-PP for Ga, In.

Table 4. Computed thermochemical reaction energies of group 13 oxyfluorides (298.15 K) in kcal/mol.

Reactions	B		Al		Ga		In	
	$\Delta E^{[a]} + \Delta ZPE^{[b]}$	$\Delta_r H$	$\Delta E^{[a]} + \Delta ZPE^{[b]}$	$\Delta_r H$	$\Delta E^{[a]} + \Delta ZPE^{[b]}$	$\Delta_r H$	$\Delta E^{[a]} + \Delta ZPE^{[b]}$	$\Delta_r H$
$M + OF_2 \rightarrow OMF_2$	−327.9	−326.0	−276.1	−275.9	−210.5	−210.6	−169.1	−169.4
$M + OF \rightarrow OMF$	−293.6	−291.7	−201.5	−201.3	−162.1	−162.0	−129.3	−129.4
$OMF_2 \rightarrow OMF + F$	72.0	72.1	112.0	112.3	85.8	86.3	77.3	77.6

[a] Energy changes (kcal/mol) for the reactions computed at the CCSD(T)/aug-cc-pVTZ-PP level. [b] Using zero-point energy corrections for the electronic energies at the CCSD(T) level.

produced by photo- or metal-induced fluorine atom abstraction from OF_2, the latter being indicated by observation of MF_n species. Furthermore, OMF molecules can also be obtained through a dissociation channel in which OMF_2 molecules release a fluorine atom [reaction (3)]. The calculated dissociation energies for the B–F, Al–F, Ga–F and In–F bonds in the OMF_2 molecules are 72.0, 112.0, 85.8 and 77.3 kcal/mol, respectively.

$$M + OF \rightarrow OMF \quad (2)$$

$$OMF_2 \rightarrow OMF + F \quad (3)$$

One of the important reactions of highly reactive radical species is usually the dimerization [reaction (4)].

$$\cdot OMF_2 + \cdot OMF_2 \rightarrow F_2M(\mu-\eta^2:\eta^2-O_2)MF_2 \quad (4)$$

From the reported detailed theoretical studies,[28] it can be concluded that all these dimers have C_{2v} geometry and show an $^1A_1$ ground state stabilized by radical-radical interactions and their dimerization processes must be exothermic. Furthermore, aluminum compound $F_2Al(\mu-\eta^2:\eta^2-O_2)AlF_2$ exhibits exceptionally high stability due to its dimerization reaction releasing more energy. Nevertheless, the formation of dimers within the matrix is usually prohibited and is not observed in our experiments.

Conclusions

In summary, we have synthesized and characterized the OMF_2 radicals for the first time by the reactions of laser-ablated group 13 atoms M (M=B, Al, Ga and In) with OF_2 in solid neon or argon matrices at 5 K. The assignments were supported by $^{16/18}O$ isotope substitution experiments as well as quantum-chemical calculations up to state-of-the-art coupled cluster level. The calculations predict the vibrational frequencies of the whole series of OMF_2 (M=B, Al, Ga, In) molecules showing planar C_{2v} structures with a $^2B_2$ ground state. These theoretical frequencies and oxygen isotopic shifts support our assignments for these molecules. The computed molecular orbitals (MOs) and spin densities of group 13 oxydifluorides OMF_2 show that the radical character is almost exclusively centered at the oxygen atoms. Moreover, the linear structures of the OMF molecules with $C_{\infty v}$ symmetry in its ground states were observed in argon during sample deposition. For the OBF molecule, two degenerate π bonds and one O→B dative σ bond constitute the triple bond character between B and O, which could be further identified by the calculated short B–O bond length and detailed NRT analysis. For the OAlF, OGaF and OInF oxo monofluorides, it is more reasonable to characterize their Al–O and Ga–O bonds as highly polar triple bonds while the In–O bond is best described by a highly polar double bond based on NRT analysis. Additionally, the reactions of the group 13 atoms with OF_2 have been computed to be highly exothermic, providing the energy for the formation of OMF molecules.

Acknowledgements

We gratefully acknowledge the Zentraleinrichtung für Datenverarbeitung (ZEDAT) of the Freie Universität Berlin for the allocation of computing resources.[56] We thank the ERC Project HighPotOx (Grant agreement ID: 818862) as well as the CRC 1349 (SFB 1349) Fluorine-Specific Interactions-Project-ID 387284271 for continuous support. M. W. thanks the China Scholarship Council (PhD Program) for financial support. Open Access funding enabled and organized by Projekt DEAL.

Conflict of Interests

The authors declare no conflict of interest.

Data Availability Statement

The data that support the findings of this study are available from the corresponding author upon reasonable request.

Keywords: Group 13 oxyfluorides · laser-ablation · matrix-isolation · multiple bonds · quantum-chemical calculations

[1] B. Halliwell, J. M. Gutteridge, *Biochem. J.* **1984**, *219*, 1–14.
[2] J. A. Imlay, S. Linn, *Science* **1988**, *240*, 1302–1309.
[3] G. Panov, K. Dubkov, E. Starokon, *Catal. Today* **2006**, *117*, 148–155.
[4] J. J. Orlando, G. S. Tyndall, T. J. Wallington, *Chem. Rev.* **2003**, *103*, 4657–4690.
[5] A. C. Davis, J. S. Francisco, *J. Am. Chem. Soc.* **2011**, *133*, 18208–18219.
[6] A. Baralle, A. Baroudi, M. Daniel, L. Fensterbank, J. -P. Goddard, E. Lacôte, M. -H. Larraufie, G. Maestri, M. Malacria, C. Ollivier *In Encyclopedia of Radicals in Chemistry, Biology and Materials* (Eds.: C. Chatgilialoglu, A. Studer), John Wiley & Sons, Ltd, Chichester, UK, **2012**.
[7] L. Chang, Q. An, L. Duan, K. Feng, Z. Zuo, *Chem. Rev.* **2022**, *122*, 2429–2486.
[8] K. J. Davies, *J. Biol. Chem.* **1987**, *262*, 9895–9901.
[9] H. Beckers, P. Garcia, H. Willner, G. A. Argüello, C. J. Cobos, J. S. Francisco, *Angew. Chem. Int. Ed.* **2007**, *46*, 3754–3757.
[10] B. Zhu, X. Zeng, H. Beckers, J. S. Francisco, H. Willner, *Angew. Chem. Int. Ed. Engl.* **2015**, *54*, 11404–11408.
[11] G. Pannetier, A. G. Gaydon, *Nature* **1948**, *161*, 242–243.
[12] E. H. Coleman, A. G. Gaydon, W. M. Vaidya, *Nature* **1948**, *162*, 108–109.
[13] A. Arkell, *J. Am. Chem. Soc.* **1965**, *87*, 4057–4062.
[14] A. Loewenschuss, J. C. Miller, L. Andrews, *J. Mol. Spectrosc.* **1980**, *80*, 351–362.
[15] K. Gobindlal, Z. Zujovic, P. Yadav, J. Sperry, C. C. Weber, *J. Phys. Chem. C.* **2021**, *125*, 20877–20886.
[16] S. Steenken, L. Goldbergerova, *J. Am. Chem. Soc.* **1998**, *120*, 3928–3934.
[17] C. Mathews, K. K. Innes, *J. Mol. Spectrosc.* **1965**, *15*, 199–210.
[18] C. Mathews, *J. Mol. Spectrosc.* **1966**, *19*, 203–223.
[19] I. Baraille, C. Larrieu, A. Dargelos, M. Chaillet, *Chem. Phys.* **2002**, *282*, 9–20.
[20] C. Puzzarini, V. Barone, *Phys. Chem. Chem. Phys.* **2008**, *10*, 6991–6997.
[21] R. Grimminger, P. M. Sheridan, D. J. Clouthier, *J. Chem. Phys.* **2014**, *140*, 164302.
[22] L. Andrews, X. F. Wang, Y. Gong, T. Schlöder, S. Riedel, M. J. Franger, *Angew. Chem. Int. Ed.* **2012**, *51*, 8235–8238.
[23] R. Wei, Z. T. Fang, M. Vasiliu, D. A. Dixon, L. Andrews, Y. Gong, *Inorg. Chem.* **2019**, *58*, 9796–9810.
[24] L. Li, T. Stüker, S. Kieninger, D. Andrae, T. Schlöder, Y. Gong, L. Andrews, H. Beckers, S. Riedel, *Nat. Common.* **2018**, *9*, 1267.
[25] Y. Gong, L. Andrews, C. W. Bauschlicher Jr., *J. Phys. Chem. A.* **2012**, *116*, 10115–10121.

[26] Y. Gong, L. Andrews, C. W. Bauschlicher Jr., *Chem. Eur. J.* **2012**, *18*, 12446–12451.
[27] L. Li, H. Beckers, T. Stüker, T. Lindič, T. Schlöder, D. Andrae, S. Riedel, *Inorg. Chem. Front.* **2021**, *8*, 1215–1228.
[28] A. Hammerl, J. Welch Barry, P. Schwerdtfeger, *Inorg. Chem.* **2004**, *43*, 1436–1440.
[29] T. Schlöder, T. Vent-Schmidt, S. Riedel, *Angew. Chem. Int. Ed.* **2012**, *51*, 12063–12067.
[30] T. Vent-Schmidt, J. Metzger, L. Andrews, S. Riedel, *J. Fluorine Chem.* **2015**, *174*, 2–7.
[31] A. H. Borning, K. E. Pullen, *Inorg. Chem.* **1969**, *8*, 1791.
[32] M. J. Frisch, G. W. Trucks, H. B. Schlegel, G. E. Scuseria, M. A. Robb, J. R. Cheeseman, G. Scalmani, V. Barone, G. A. Petersson, H. Nakatsuji, X. Li, M. Caricato, A. V. Marenich, J. Bloino, B. G. Janesko, R. Gomperts, B. Mennucci, H. P. Hratchian, J. V. Ortiz, A. F. Izmaylov, J. L. Sonnenberg, D. Williams-Young, F. Ding, F. Lipparini, F. Egidi, J. Goings, B. Peng, A. Petrone, T. Henderson, D. Ranasinghe, V. G. Zakrzewski, J. Gao, N. Rega, G. Zheng, W. Liang, M. Hada, M. Ehara, K. Toyota, R. Fukuda, J. Hasegawa, M. Ishida, T. Nakajima, Y. Honda, O. Kitao, H. Nakai, T. Vreven, K. Throssell, J. A. Montgomery, Jr., J. E. Peralta, F. Ogliaro, M. J. Bearpark, J. J. Heyd, E. N. Brothers, K. N. Kudin, V. N. Staroverov, T. A. Keith, R. Kobayashi, J. Normand, K. Raghavachari, A. P. Rendell, J. C. Burant, S. S. Iyengar, J. Tomasi, M. Cossi, J. M. Millam, M. Klene, C. Adamo, R. Cammi, J. W. Ochterski, R. L. Martin, K. Morokuma, O. Farkas, J. B. Foresman, D. J. Fox, *Gaussian 16*, Gaussian, Inc., Wallingford CT, **2016**.
[33] S. Grimme, J. Antony, S. Ehrlich, H. Krieg, *J. Chem. Phys.* **2010**, *132*, 154104.
[34] S. Grimme, S. Ehrlich, L. Goerigk, *J. Comput. Chem.* **2011**, *32*, 1456–1465.
[35] F. Neese, A. Hansen, D. G. Liakos, *J. Chem. Phys.* **2009**, *131*, 64103.
[36] G. D. Purvis, R. J. Bartlett, *J. Chem. Phys.* **1982**, *76*, 1910–1918.
[37] K. Raghavachari, G. W. Trucks, J. A. Pople, M. Head-Gordon, *Chem. Phys. Lett.* **1989**, *157*, 479–483.
[38] R. A. Kendall, T. H. Dunning, R. J. Harrison, *J. Chem. Phys.* **1992**, *96*, 6796–6806.
[39] K. A. Peterson, D. Figgen, M. Dolg, H. Stoll, *J. Chem. Phys*. **2007**, *126*, 124101.
[40] D. Figgen, K. A. Peterson, M. Dolg, H. Stoll, *J. Chem. Phys.* **2009**, *130*, 164108.
[41] E. D. Glendening, J. K. Badenhoop, A. E. Reed, J. E. Carpenter, J. A. Bohmann, C. M. Morales, P. Karafiloglou, C. R. Landis, F. Weinhold, *NBO 7.0*, Theoretical Chemistry Institute, University of Wisconsin, Madison, WI, **2018**.
[42] G. A. Zhurko, Chemcraft - graphical program for visualization of quantum chemistry computations, Ivanovo (Russia), **2005** http://www.chemcraftprog.com.
[43] M. E. Jacox, W. E. Thompson, *J. Chem. Phys.* **1995**, *102*, 4747–4756.
[44] T. R. Burkholder, L. Andrews, *J. Chem. Phys.* **1991**, *95*, 8697–8709.
[45] X. F. Wang, L. Andrews, *J. Am. Chem. Soc.* **2011**, *133*, 3768–3771.
[46] H. Schnöckel, *J. Mol. Struct.* **1978**, *50*, 267–273.
[47] H. Schnöckel, H. J. Goecke, *J. Mol. Struct.* **1978**, *50*, 281–284.
[48] A. Köhn, B. Gaertner, H.-J. Himmel, *Chem. Eur. J.* **2005**, *11*, 5575–5588.
[49] D. G. Hall, *Boronic Acids*, Wiley, **2005**.
[50] A. R. Barron, K. D. Dobbs, M. M. Francl, *J. Am. Chem. Soc.* **1991**, *113*, 39–43.
[51] H. Braunschweig, K. Radacki, A. Schneider, *Science* **2010**, *328*, 345–347.
[52] H. Bock, L. Cederbaum, W. von Niessen, P. Paetzold, P. Rosmus, B. Solouki, *Angew. Chem. Int. Ed. Engl.* **1989**, *28*, 88–90.
[53] D. K. Straub, *J. Chem. Educ.* **1995**, *72*, 494.
[54] M. D. Anker, M. P. Coles, *Angew. Chem. Int. Ed. Engl.* **2019**, *58*, 18261–18265.
[55] H. Siebert, *Anwendungen der Schwingungsspektroskopie in der Anorganischen Chemie*, Springer Berlin Heidelberg, **1966**.
[56] L. Bennett, B. Melchers, B. Proppe, *Freie Universität Berlin*, **2020**, DOI: 10.17169/refubium-26754.

Manuscript received: May 26, 2023
Accepted manuscript online: June 20, 2023
Version of record online: August 1, 2023